ADVANCED OPTICAL MATERIALS
www.advopticalmat.de

A Red-Emissive Fluorescent Probe with a Compact Single-Benzene-Based Skeleton for Cell Imaging of Lipid Droplets

Ri Zhou, Yuanyuan Cui, Jianan Dai, Chenguang Wang, Xishuang Liang, Xu Yan, Fangmeng Liu, Xiaomin Liu, Peng Sun, Hongyu Zhang, Yue Wang, and Geyu Lu**

Lipid droplets (LDs) are important organelles associated with many physiological processes as well as diseases. To visualize LDs and study their versatile functions, the fluorescence imaging technique is one of the most powerful tools. Thus, the development of fluorescent probes for LDs imaging has attracted increased attention in recent years. Herein, a new LDs fluorescent probe Ph-Red is developed and its application in fluorescence imaging is carefully demonstrated. The probe Ph-Red has a compact single-benzene-based molecular structure and can be easily synthesized via a one-step reaction. Impressively, the probe displays strong red emission based on a very small π-system consisting of only one benzene ring. Moreover, the probe shows high LDs staining selectivity and good cellular viability, and is tolerant for repeatedly fluorescence imaging. Given these advantages, the 3D confocal imaging in fixed cells as well as multicolor confocal imaging in live cells are successfully realized, highlighting the utility of the single-benzene-based fluorescent probe Ph-Red for LDs imaging. In addition, the hydrophobicity of the probe and the molecular size are revealed to play critical roles for efficiently staining LDs, which are important insights for the development of new LDs fluorescent probes.

1. Introduction

Lipid droplets (LDs) are spherical organelles which consist of a core of neutral lipids such as triglycerides and cholesterol esters, and a surrounding membrane of phospholipid monolayer anchored with proteins. LDs which exist in almost all organisms from prokaryotes to humans play pivotal roles in not only the storage of lipid,[1–3] but also in various other cellular events including membrane trafficking,[4] protein storage,[5] and inflammation.[6] Moreover, LDs are strongly relative to some diseases, such as neurodegeneration,[7] obesity,[8] and cancer.[9]

To visualize LDs and study their versatile functions, the fluorescence imaging technique is one of the most powerful tools. Currently, BODIPY 493/503 and Nile Red are commonly used fluorescent probes for LDs fluorescence imaging (**Scheme 1**a).[10] However, these two probes have several weaknesses. For example, BODIPY 493/503 displays a small Stokes shift that causes cross-talk between the excitation source and the fluorescence emission; Nile Red stains LDs as well as other hydrophobic structures resulting in a low LDs selectivity and an unfavorable signal-to-noise ratio.[10]

In this context, the development of superior fluorescent probes for LDs imaging has attracted increased attention in recent years.[10–27] For example, Tang and co-workers reported a donor–acceptor type blue-emissive probe TPA-BI which is capable for two-photon imaging of LDs (Scheme 1b).[11] Yamaguchi and co-workers developed a green-emissive LDs probe LipiDye which has been successfully commercialized.[12,13] Collot and co-workers reported a series of merocyanine-based probes SMCy which display yellow to the near-infrared emissions with high brightness and fluorogenic character.[14] These works significantly advance the imaging and study of LDs. Nonetheless, the species of LDs fluorescent probes are still relatively limited. Moreover, the molecular structures of these LDs probes are somewhat complicated and required tedious chemical synthesis.

To develop new LDs fluorescent probe, we focus on the π-conjugated skeleton with compact molecular structure, even single-benzene π-system. Featuring with simple molecular structure as well as simple synthetic procedure, several single-benzene-based fluorophores have been developed by Katagiri's group,[28] Yuan's group,[29] Fang's group,[30] our group,[31–36] and others.[37–41] Dimethyl 2,5-bis(methylamino)terephthalate (compound **1**, Scheme 1c) is a representative single-benzene fluorophore reported by us in 2017.[31] With a very small single-benzene π-system, this compound impressively displays intense red emission in crystals. Employing the derivatives of this compound, we subsequently developed the functional

R. Zhou, J. Dai, Prof. C. Wang, Prof. X. Liang, Prof. X. Yan, Prof. F. Liu, Prof. X. Liu, Prof. P. Sun, Prof. G. Lu
State Key Laboratory on Integrated Optoelectronics
Key Laboratory of Advanced Gas Sensors, Jilin Province
College of Electronic Science and Engineering
Jilin University
2699 Qianjin Street, Changchun 130012, China
E-mail: wangchenguang@jlu.edu.cn; lugy@jlu.edu.cn
Y. Cui, Prof. H. Zhang, Prof. Y. Wang
State Key Laboratory of Supramolecular Structure and Materials
College of Chemistry
Jilin University
2699 Qianjin Street, Changchun 130012, China
The ORCID identification number(s) for the author(s) of this article can be found under https://doi.org/10.1002/adom.201902123.

DOI: 10.1002/adom.201902123

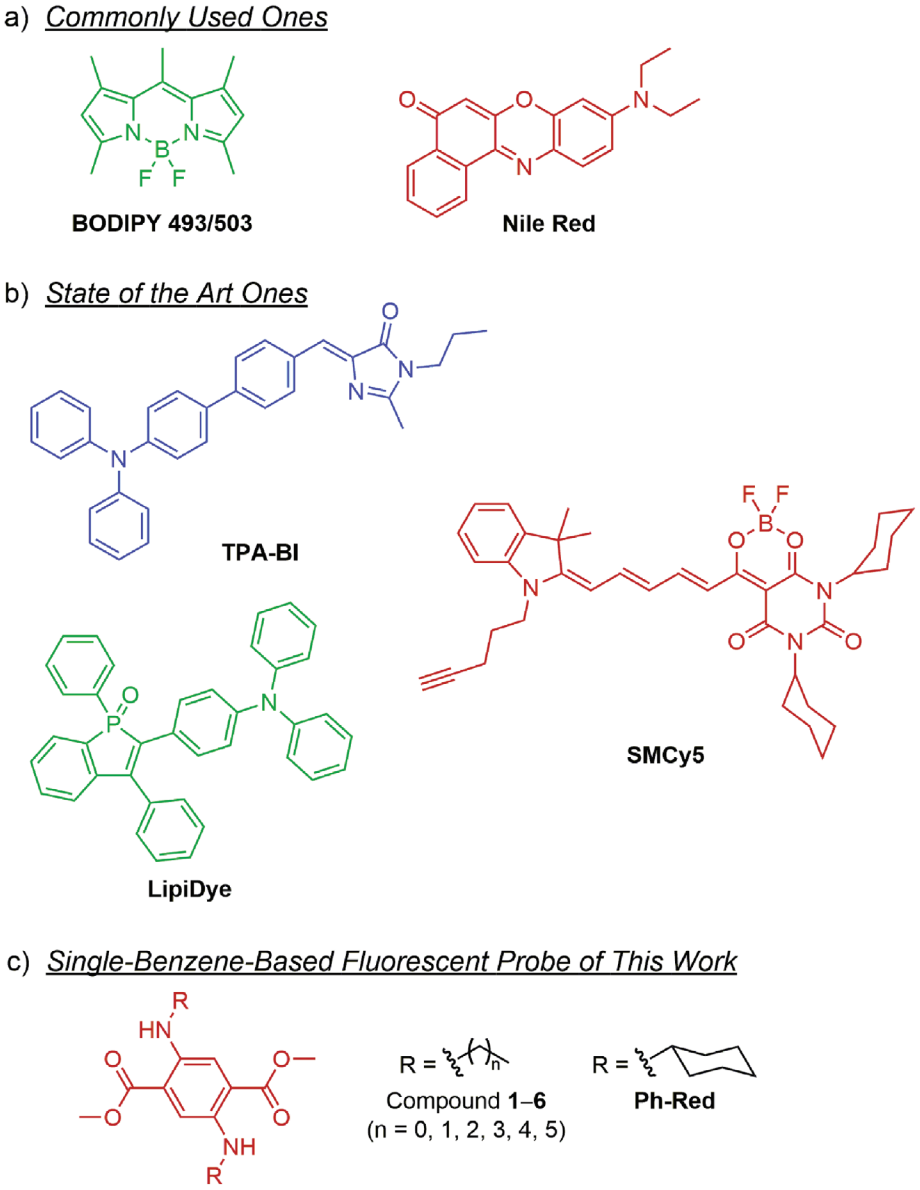

Scheme 1. Molecular structures of lipid droplets (LDs) fluorescent probes. The color of each probe indicates its emission color (blue, green, or red).

organic crystals which can be reversibly bent under mechanical force and are potentially applied in flexible optical devices.[32,33]

Herein, we explore the cell imaging application of this red-emissive single-benzene fluorophore, and thus newly develop a LDs fluorescent probe Ph-Red with two cyclohexyl substituents (Scheme 1c). Besides simple molecular structure and synthesis, the single-benzene-based fluorescent probe Ph-Red displays favorable absorption and emission properties for LDs fluorescence imaging, such as strong red emission, large Stokes shift, and capable for the commonly used 488 nm excitation laser. Moreover, this probe displays higher LDs staining selectivity in cells than the commonly used BODIPY 493/503 and Nile Red. Given these advantages of Ph-Red, we successfully realized 3D confocal imaging in fixed cells as well as multicolor confocal imaging in live cells, highlighting utility of this single-benzene-based fluorescent probe for LDs imaging. In addition, we reveal that both the hydrophobicity of probe and the molecular size play critical roles for efficiently staining LDs, which are important insights for development of new LDs fluorescent probes.

2. Results and Discussion

2.1. Synthesis

The synthesis of probe Ph-Red is very easy (**Scheme 2**). One-step condensation between dimethyl 1,4-cyclohexanedione-2,5-dicarboxylate and cyclohexylamine under air atmosphere readily produced Ph-Red in 54% yield. The molecular structure of Ph-Red was characterized by ^{1}H and ^{13}C NMR spectra, and further confirmed by single-crystal X-ray diffraction analysis.

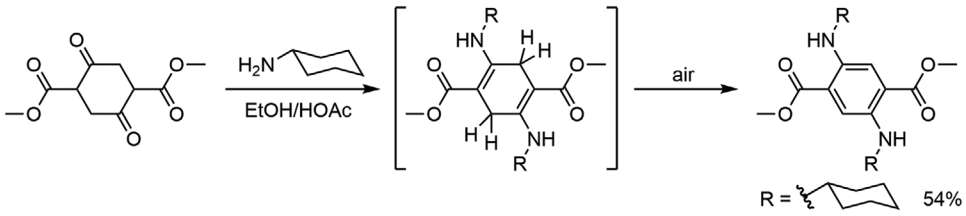

Scheme 2. Synthesis of the single-benzene-based fluorescent probe Ph-Red.

In a similar manner, compounds **1–6** (Scheme 1c) with various alkyl chains were also synthesized for comparison of cellular staining property (Supporting Information).

2.2. Photophysical Properties

The photophysical properties of single-benzene-based fluorescent probe Ph-Red were investigated in various solvents (**Figure 1** and **Table 1**). The absorption (λ_{abs}) and emission (λ_{em}) maxima are around 490 and 600 nm, respectively, which are insensitive to the solvent polarity. While featuring a large Stokes shift of about 110 nm, this probe displays intense red emission with a fluorescence quantum yield (Φ_F) of about 0.30 in solution. The fluorescence brightness of Ph-Red, as determined by $\varepsilon \times \Phi_F$, is about 1500 M^{-1} cm^{-1}. This value is well in comparison to the representative dyes with large Stokes, e.g. Lucifer Yellow CH[42] and Star 470SXP.[43] The very small single-benzene π-system displaying such long-wavelength absorption and emission, large Stokes shift as well as good brightness is really unusual. The unique photophysical properties endow Ph-Red with the following advantages for fluorescence imaging: 1) the long-wavelength emission is highly appreciated because the auto-fluorescence background signal of cells which are generally in short-wavelength range can be significantly diminished; 2) the large Stokes shift could effectively avoid the cross-talk between the excitation source and the detection of fluorescence; 3) the absorption of probe is quite suitable for the commonly used 488 nm excitation laser of fluorescence microscopy. Besides of solutions, the probe Ph-Red also displays intense red emission (λ_{em} = 628 nm) with a Φ_F of 0.27 in solid state (Figure 1). Thus, this probe does not encounter the bottleneck of aggregation-caused fluorescence quenching (ACQ), and can be used in high concentration or even in solid state (nanoparticles) for fluorescence imaging.

2.3. LDs Staining Properties

We first conducted co-staining experiments of LDs in living HeLa cells (**Figure 2**). The cells were stained with BODIPY 493/503 (2×10^{-6} M) and Ph-Red (500×10^{-9} M) for 1 h, and were imaged in green channel (λ_{ex} = 488 nm, λ_{em} = 500–540 nm) and red channel (λ_{ex} = 488 nm; λ_{em} = 600–640 nm), respectively. The two channels are well overlapped with each other, and a high Pearson's *R* value of 0.85 is observed (Figure S2, Supporting Information). This result indicates the well LDs selectivity of the single-benzene-based fluorescent probe Ph-Red.

We next carefully studied the cellular staining property of probe Ph-Red. The live HeLa cells were stained with Ph-Red, BODIPY 493/503, or Nile Red in various concentrations (200×10^{-9} M, 1×10^{-6} M, and 5×10^{-6} M) for 1 h. It was found that Ph-Red could efficiently stain LDs with high selectivity in all of these concentrations (**Figure 3**). In contrast, BODIPY 493/503 and Nile Red displayed much lower LDs selectivity, staining other cellular structures as well. This comparison strongly highlights the advantage of Ph-Red. The cell viability of Ph-Red was also evaluated by MTT assay (Figure S3, Supporting Information). With a concentration up to 5×10^{-6} M, the probe did not affect the cell viability within 24 h. These results

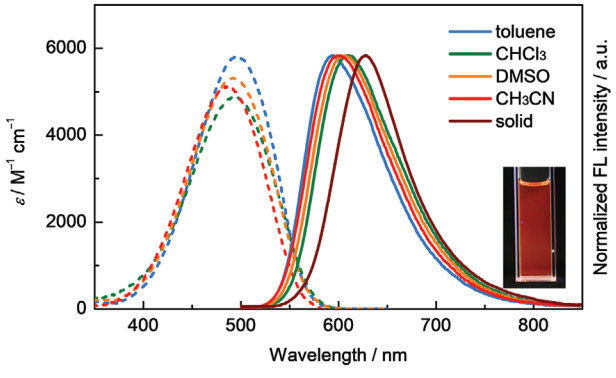

Figure 1. Absorption (dashed line) and fluorescence (solid line) spectra of the probe Ph-Red in various organic solvents, and its fluorescence spectrum in solid state. Inset: the photograph of its $CHCl_3$ solution under UV light.

Table 1. Photophysical data for the probe Ph-Red.

Probe	Solution or solid	λ_{abs} [nm][a)]	ε [M^{-1} cm^{-1}]	λ_{em} [nm]	Φ_F[b)]	Brightness [M^{-1} cm^{-1}][c)]
Ph-Red	Toluene	496	5800	594	0.29	1700
	$CHCl_3$	494	4870	610	0.31	1500
	DMSO	493	5310	605	0.31	1600
	CH_3CN	487	5130	600	0.31	1600
	Solid	–	–	628	0.27	–
Lucifer Yellow CH	H_2O	428	11 300	540	0.21	2400
Star 470SXP	PBS buffer	472	29 000	624	0.12	3500

[a)]The longest wavelength absorption maximum.; [b)]Absolute fluorescence quantum yield determined by a calibrated integrating sphere system.; [c)]The brightness was determined as $\varepsilon \times \Phi_F$.

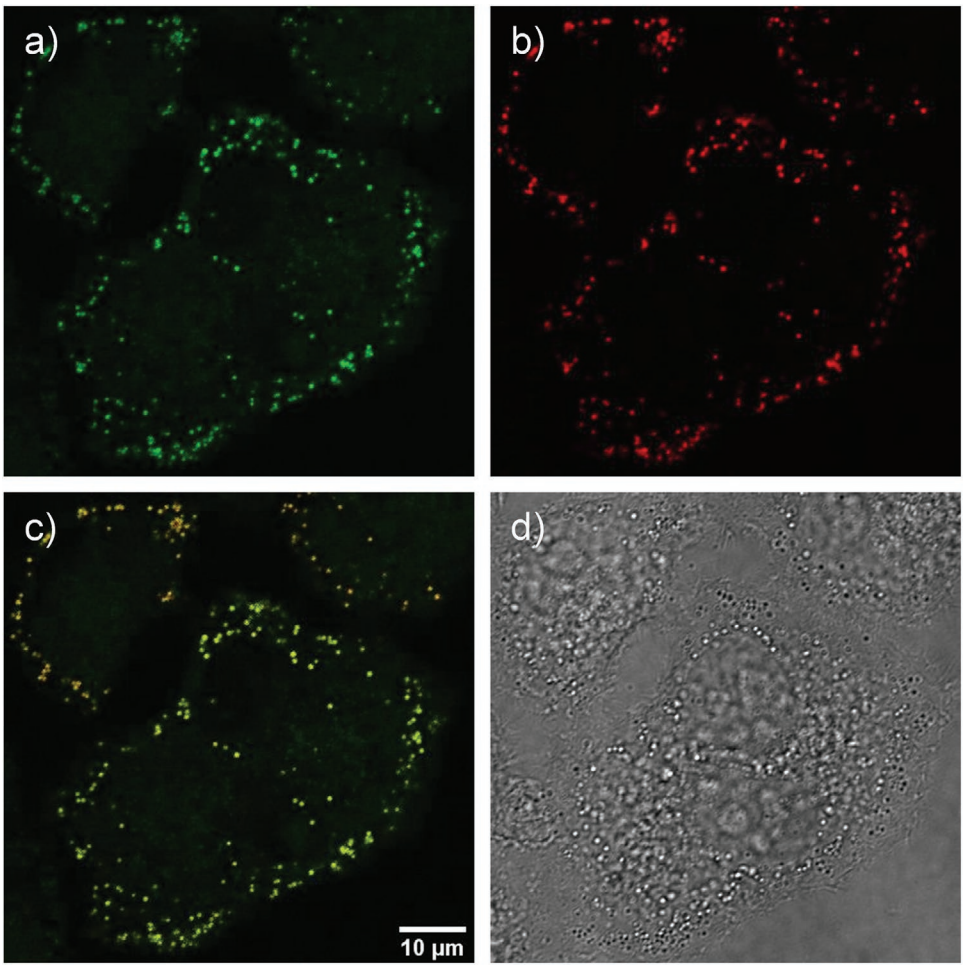

Figure 2. Colocalization confocal imaging of living HeLa cells stained with Rh-Red and BODIPY 493/503: a) imaging channel of BODIPY 493/503 (λ_{ex} = 488 nm; λ_{em} = 500–540 nm); b) imaging channel of Rh-Red (λ_{ex} = 488 nm; λ_{em} = 600–640 nm); c) merged image; d) bright field image. Scale bar: 10 μm.

demonstrate that a wide working concentration range of 200×10^{-9}–5×10^{-6} M can be adopted for the probe.

For the practical use of probe Ph-Red, a low concentration of 200×10^{-9} M is enough to get sufficient and persistent fluorescence signals even for repeatedly imaging. In fact, the LDs stained with 200×10^{-9} M of Ph-Red for 1 h provide comparable or even higher brightness than those stained with BODIPY 493/503 or Nile Red (200×10^{-9} M, 1 h) under the identical imaging condition (Figure S4, Supporting Information). The photostability of probe Ph-Red was evaluated by repeatedly recording confocal images in the same area (**Figure 4**, Movie S1 in Supporting Information). In this experiment, the HeLa cells were stained with probe Ph-Red in a low concentration of 200×10^{-9} M for 1 h. After washing out the free probe, the confocal images were recorded by a Nikon A1RMP microscope. Under the excitation of 488 nm laser, the probe Ph-Red displayed good photostability. After repeatedly recording 100 images, the fluorescence signal of probe still maintains above 80% of its initial value. Notably, the observed weak photobleaching can be significantly suppressed by increasing the probe concentration and accordingly decreasing the power of excitation laser.

The chemical stability of probe Ph-Red was evaluated in the aqueous mixture of PBS/DMSO (V/V = 3/7). As shown in Figure S5 (Supporting Information), the absorption spectra of probe Ph-Red almost did not change within 24 h in the mixture of PBS–DMSO, demonstrating the good chemical stability of this probe. The good photo- and chemical-stability of probe Ph-Red are highly desired for long-term fluorescence imaging.

The comparison of cellular staining property between Ph-Red and its analogous compounds **1–6** with various alkyl chains provides important insights for development of new LDs fluorescent probes. The live HeLa cells stained with these dyes (1×10^{-6} M, 1 h) were imaged under the identical excitation and detection (**Figure 5**). Compounds **1–2** did not provide any detectable fluorescence signal, and compound **3** could give very weak signal. For compounds **4–5**, dramatically increased fluorescence signals were observed. However, for further elongation of alkyl chains to compound **6**, the fluorescence signal was decreased. The intensity variation of fluorescence signals of compounds **1–6** strongly reveals that the alkyl chains which control the hydrophobicity of compounds largely affect the LDs staining property. To quantitatively evaluate the hydrophobicity,

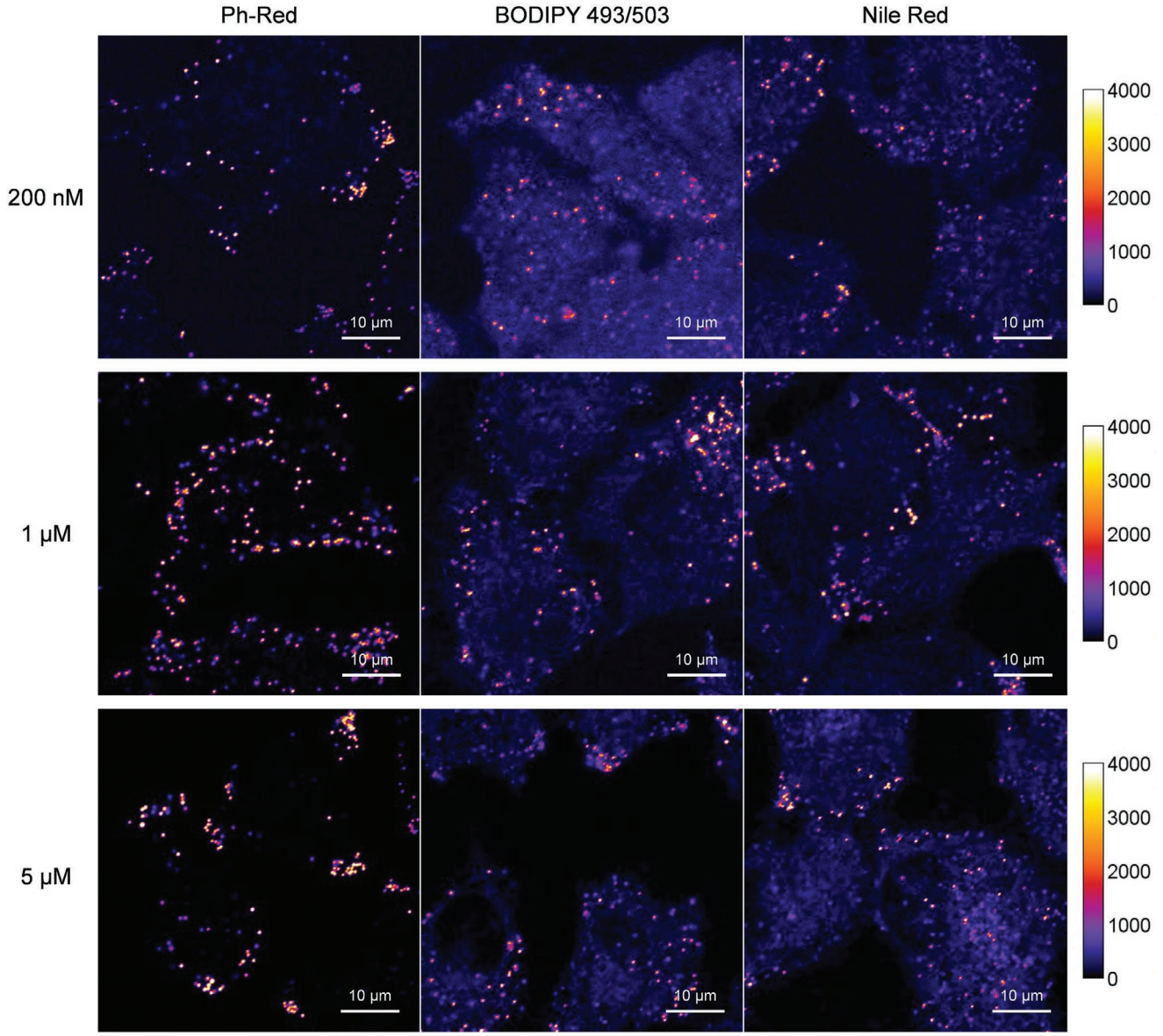

Figure 3. Comparison of the cellular staining selectivity of Ph-Red, BODIPY 493/503, and Nile Red (200×10^{-9} M, 1×10^{-6} M, or 5×10^{-6} M for 1 h) in living HeLa cells. Scale bar: 10 μm.

the CLogP which means the *n*-octanol–water partition coefficient calculated by ChemDraw is employed. Because compounds **1–6** have the identical skeleton and the only difference between them is the alkyl chain, the change in tendency of CLogP values of these compounds can be predicted by ChemDraw. On the other hand, the calculated CLogP that is usually far away from the experimental value, may be not reliable for the comparison of the compounds with different skeletons. The CLogP values of compounds **1–6** are 2.5, 3.6, 4.7, 5.7, 6.8, and 7.8, respectively. Therefore, a CLogP value of about 6 should be desired for staining LDs. Lower hydrophobicity may decrease the driving force to stain LDs, while higher hydrophobicity may decrease the cell permeability. In terms of hydrophobicity, Ph-Red which has a CLogP value of 6.6 is very reasonable for efficiently staining LDs. Moreover, Ph-Red provides much stronger fluorescence signal than compound **5** although their hydrophobicity is very similar. This result reveals that the cycloalkyl group which has a smaller spatial size than the linear alkyl group provides better cell permeability.

2.4. 3D Confocal Imaging

The 3D confocal imaging is a powerful tool to directly visualize the spatial distribution of subcellular structures. In general, the 3D image is obtained by reconstruction of Z-stack slices which involve multiple imaging scans of the sample and lead to significant photo-bleaching of the fluorescent probe. Therefore, the high brightness and the good photostability of probe are highly appreciated for 3D imaging.

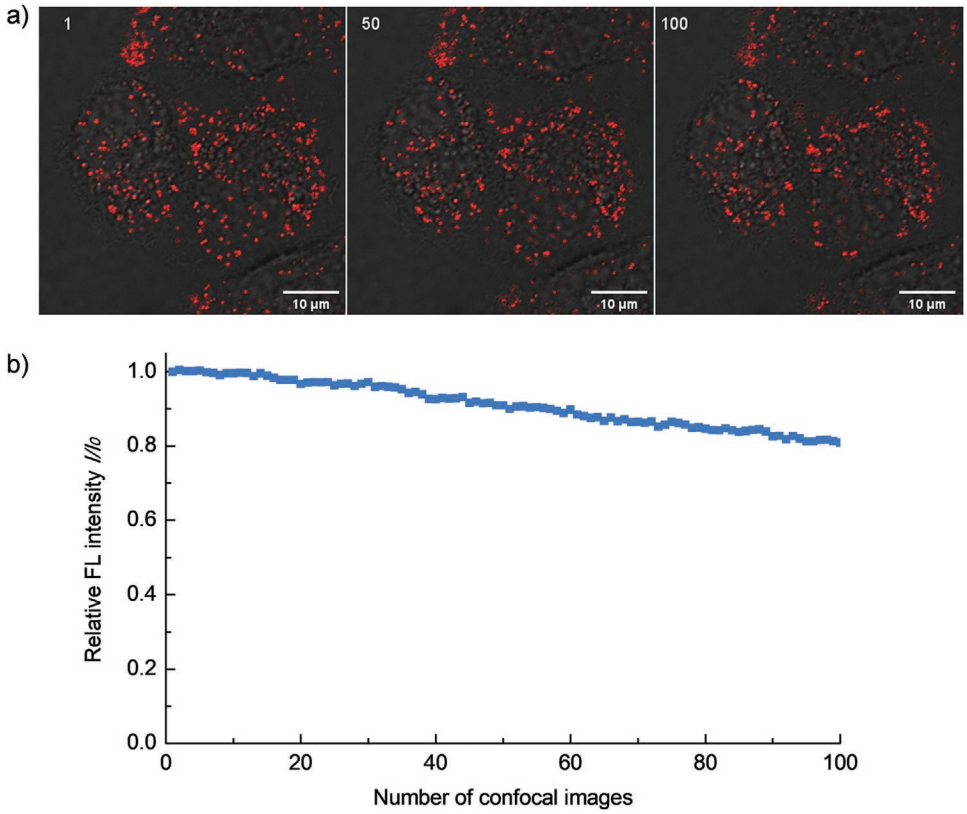

Figure 4. Repeatedly recorded confocal images of lipid droplets (LDs) stained with probe Ph-Red (200×10^{-9} M, 1 h) in the same area: a) the confocal images of number 1, 50, and 100; b) the fluorescence intensity of each image (I) relative to the initial value (I_0) plotted as a function of the recorded number. Scale bar: 10 μm.

We herein demonstrate the probe Ph-Red for this application. In consideration of that the quick movement of LDs in living cells would dramatically decrease the resolution of 3D image during recording Z-stack slices, we employed fixed cells for 3D imaging. The live HeLa cells were stained with 200×10^{-9} M Ph-Red for 1 h followed by fixing with 4% paraformaldehyde. The cell nuclei were then stained with Hoechst 33 342. The LDs and nuclei could be imaged in two channels separately. In order to get high spatial resolution as well as high contrast of 3D image, the Z-stack slices were recorded under a quite precise condition: a high xy pixel resolution of 67 nm, a small z-step of 100 nm, and a line average of 3 times per slice. Based on the 71 slices (in total 213 scans) in a z-depth of 7 μm, the two-color 3D image was successfully reconstructed with high quality (**Figure 6**, Movie S2, Supporting Information). The spatial distribution of LDs relative to the nucleus can be clearly visualized. Moreover, the full width at half maximum (FWHM) resolution of the 3D image is about 230 nm in xy plane and 420 nm in *z*-axis (Figures S6 and S7, Supporting Information), which is almost the limitation of confocal microscopy, strongly highlighting the quality of the 3D image.

2.5. Multicolor Confocal Imaging

The multicolor confocal imaging allows revealing different cellular processes on the same image and thus provides important information. We herein demonstrate the utility of probe Ph-Red in four-color confocal imaging. The nucleus, lysosomes, LDs, and mitochondria of living HeLa cells were stained with Hoechst 33 342 (blue-emissive), LysoTracker Green, Ph-Red, and MitoTracker Deep Red FM, respectively. Based on the differences of their absorption and emission spectra, the probes could be selectively detected via a line-by-line sequential scanning of four channels without cross-talk (**Figure 7**, Figure S8, Supporting Information). Thus, the four-color confocal image was successfully obtained.

3. Conclusion

We have developed a new LDs fluorescent probe Ph-Red with a compact single-benzene-based skeleton. Besides of simple molecular structure as well as simple synthetic procedure, this probe displays favorable properties for LDs fluorescence imaging, such as strong red emission, large Stokes shift, high LDs staining selectivity, good cellular viability, and tolerant for repeatedly fluorescence imaging. Given these advantages, the 3D confocal imaging in fixed cells as well as multicolor confocal imaging in live cells have been successfully realized, highlighting utility of the probe Ph-Red for LDs imaging. Further development of new single-benzene-based fluorescent probes for other cellular organelles is ongoing in our lab.

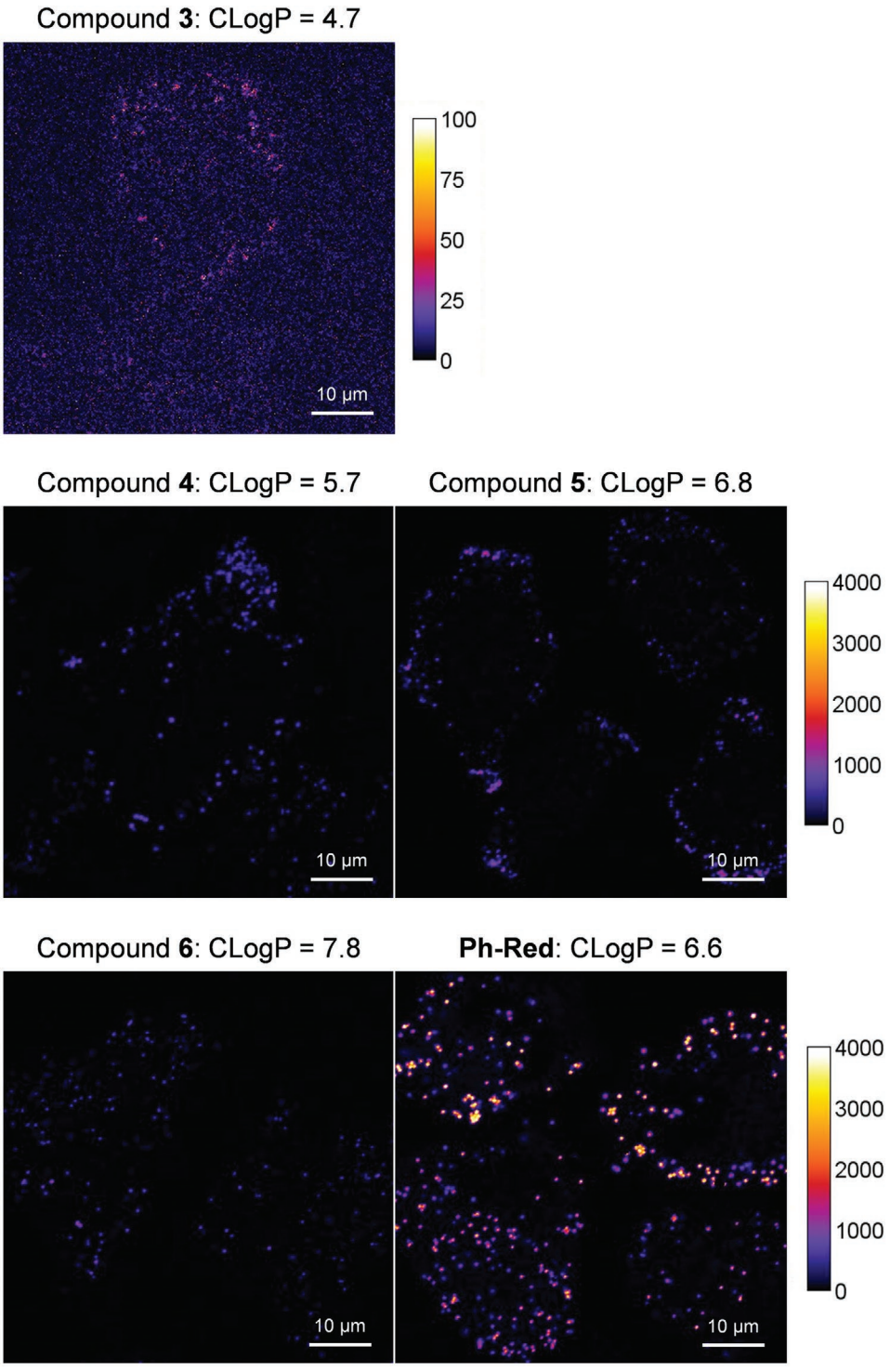

Figure 5. Comparison of the cellular staining properties of Ph-Red and compounds **3–6** in living HeLa cells under the same staining (1×10^{-6} M, 1 h) and imaging condition. Calibration bar: 0–100 for compound **3**, 0–4000 for others. Scale bar: 10 μm.

Supporting Information

Supporting Information is available from the Wiley Online Library or from the author.

Acknowledgements

This work was supported by the Science and Technology Development Program of Jilin Province (No. 20170520162JH), the National Key

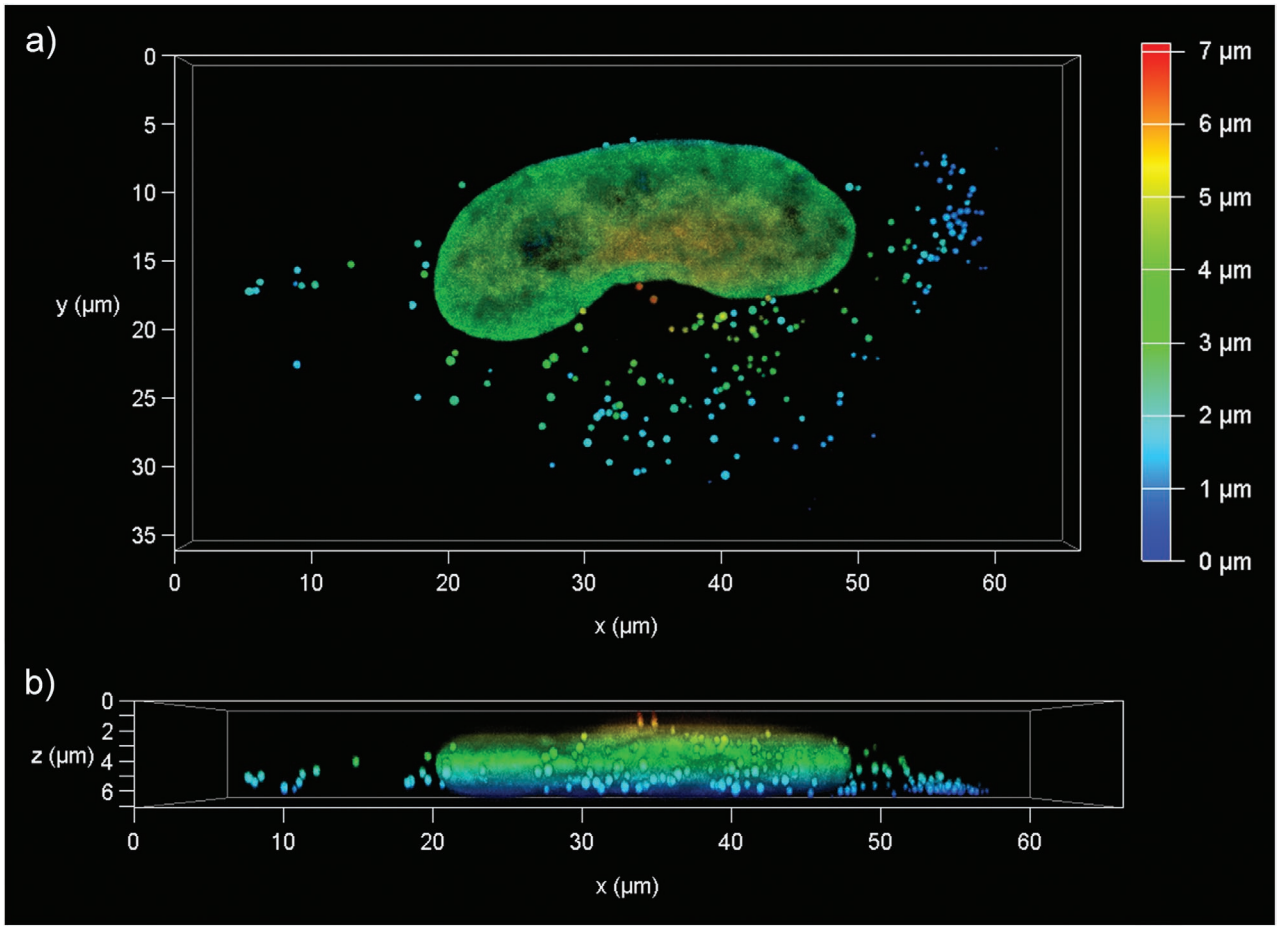

Figure 6. 3D confocal imaging of fixed HeLa cells stained with lipid droplets (LDs) probe Ph-Red and nuclei probe Hoechst 33 342: a,b) top and side views of LDs together with nuclei. The variation of color from blue to red means the different *z*-depth.

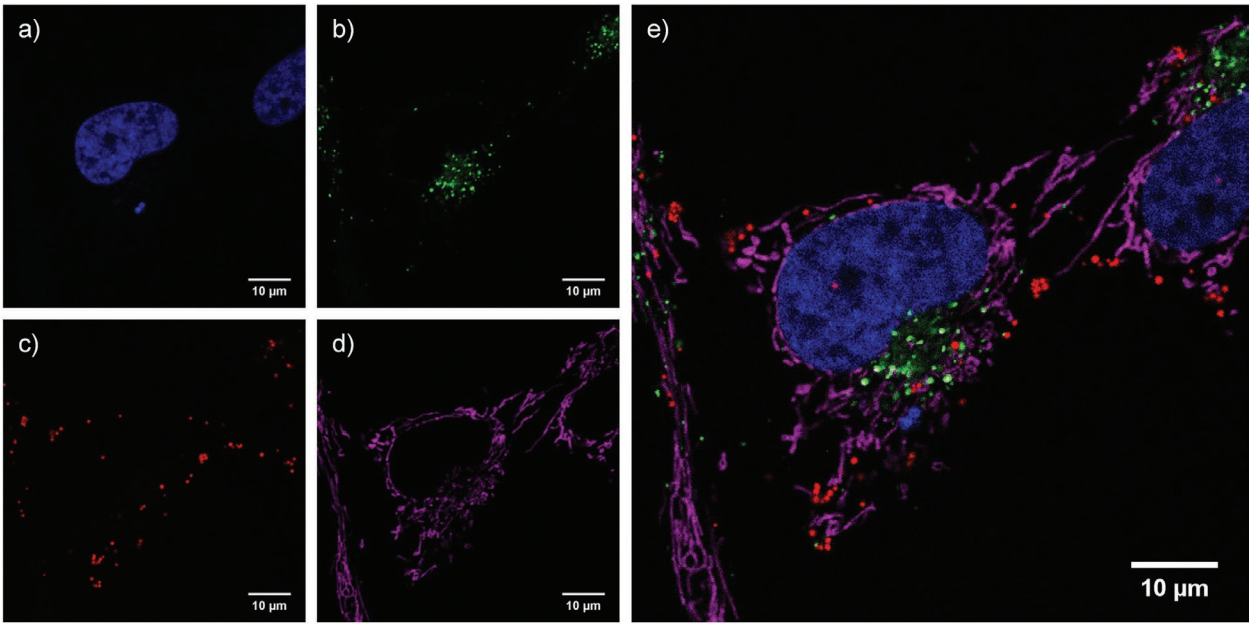

Figure 7. Multicolor confocal imaging of living HeLa cells: a) nucleus stained with Hoechst 33 342; b) lysosomes stained with LysoTracker Green; c) lipid droplets (LDs) stained with Ph-Red; d) mitochondria stained with MitoTracker Deep Red FM; and e) merged image of four channels. Scale bar: 10 μm.

Research and Development Program of China (No. 2016YFC0207300), the National Nature Science Foundation of China (Nos. 61831011, 61722305, 61833006, and 61875191), Program for JLU Science and Technology Innovative Research Team (JLUSTIRT 2017TD-07), and the Open Project of State Key Laboratory of Supramolecular Structure and Materials (sklssm202023).

Conflict of Interest

The authors declare no conflict of interest.

Keywords

fluorescence imaging, fluorescent probes, fluorophores, lipid droplets, organic dyes

Received: December 19, 2019
Revised: March 16, 2020
Published online: May 4, 2020

[1] A. R. Thiam, R. V. Farese Jr, T. C. Walther, *Nat. Rev. Mol. Cell Biol.* **2013**, *14*, 775.
[2] T. C. Walther, R. V. Farese Jr, *Annu. Rev. Biochem.* **2012**, *81*, 687.
[3] S. Martin, R. G. Parton, *Nat. Rev. Mol. Cell Biol.* **2006**, *7*, 373.
[4] J. K. Zehmer, Y. Huang, G. Peng, J. Pu, R. G. W. Anderson, P. Liu, *Proteomics* **2009**, *9*, 914.
[5] Z. Li, K. Thiel, P. J. Thul, M. Beller, R. P. Kühnlein, M. A. Welte, *Curr. Biol.* **2012**, *22*, 2104.
[6] P. T. Bozza, J. P. B. Viola, *Prostaglandins, Leukotrienes Essent. Fatty Acids* **2010**, *82*, 243.
[7] L. Liu, K. Zhang, H. Sandoval, S. Yamamoto, M. Jaiswal, E. Sanz, Z. Li, J. Hui, B. H. Graham, A. Quintana, *Cell* **2015**, *160*, 177.
[8] B. M. Spiegelman, J. S. Flier, *Cell* **2001**, *104*, 531.
[9] L. Tirinato, F. Pagliari, T. Limongi, M. Marini, A. Falqui, J. Seco, P. Candeloro, C. Liberale, E. Di Fabrizio, *Stem Cells Int.* **2017**, *2017*, 1656053.
[10] T. Fam, A. Klymchenko, M. Collot, *Materials* **2018**, *11*, 1768.
[11] M. Jiang, X. Gu, J. W. Y. Lam, Y. Zhang, R. T. K. Kwok, K. S. Wong, B. Z. Tang, *Chem. Sci.* **2017**, *8*, 5440.
[12] E. Yamaguchi, C. Wang, A. Fukazawa, M. Taki, Y. Sato, T. Sasaki, M. Ueda, N. Sasaki, T. Higashiyama, S. Yamaguchi, *Angew. Chem., Int. Ed.* **2015**, *54*, 4539.
[13] Funakoshi, Frontiers in Life Science, http://www.funakoshi.co.jp/exports_contents/80682 (accessed: January 2018).
[14] M. Collot, T. K. Fam, P. Ashokkumar, O. Faklaris, T. Galli, L. Danglot, A. S. Klymchenko, *J. Am. Chem. Soc.* **2018**, *140*, 5401.
[15] M. Collot, S. Bou, T. K. Fam, L. Richert, Y. Mély, L. Danglot, A. S. Klymchenko, *Anal. Chem.* **2019**, *91*, 1928.
[16] L. Shi, K. Li, L.-L. Li, S.-Y. Chen, M.-Y. Li, Q. Zhou, N. Wang, X.-Q. Yu, *Chem. Sci.* **2018**, *9*, 8969.
[17] D. Dang, H. Liu, J. Wang, M. Chen, Y. Liu, H. H.-Y. Sung, I. D. Williams, R. T. K. Kwok, J. W. Y. Lam, B. Z. Tang, *Chem. Mater.* **2018**, *30*, 7892.
[18] D. Wang, H. Su, R. T. K. Kwok, G. Shan, A. C. S. Leung, M. M. S. Lee, H. H. Y. Sung, I. D. Williams, J. W. Y. Lam, B. Z. Tang, *Adv. Funct. Mater.* **2017**, *27*, 1704039.
[19] M. Gao, H. Su, S. Li, Y. Lin, X. Ling, A. Qin, B. Z. Tang, *Chem. Commun.* **2017**, *53*, 921.
[20] M. Gao, H. Su, Y. Lin, X. Ling, S. Li, A. Qin, B. Z. Tang, *Chem. Sci.* **2017**, *8*, 1763.
[21] M. Kang, X. Gu, R. T. Kwok, C. W. Leung, J. W. Lam, F. Li, B. Z. Tang, *Chem. Commun.* **2016**, *52*, 5957.
[22] Z. Wang, C. Gui, E. Zhao, J. Wang, X. Li, A. Qin, Z. Zhao, Z. Yu, B. Z. Tang, *ACS Appl. Mater. Interfaces* **2016**, *8*, 10193.
[23] Y. Tatenaka, H. Kato, M. Ishiyama, K. Sasamoto, M. Shiga, H. Nishitoh, Y. Ueno, *Biochemistry* **2019**, *58*, 499.
[24] H. Appelqvist, K. Stranius, K. Börjesson, K. P. R. Nilsson, C. Dyrager, *Bioconjugate Chem.* **2017**, *28*, 1363.
[25] H. Kim, A. Jo, J. Ha, Y. Lee, Y. S. Hwang, S. B. Park, *Chem. Commun.* **2016**, *52*, 7822.
[26] E. Kim, S. Lee, S. B. Park, *Chem. Commun.* **2012**, *48*, 2331.
[27] A. Goel, A. Sharma, M. Kathuria, A. Bhattacharjee, A. Verma, P. R. Mishra, A. Nazir, K. Mitra, *Org. Lett.* **2014**, *16*, 756.
[28] T. Beppu, K. Tomiguchi, A. Masuhara, Y.-J. Pu, H. Katagiri, *Angew. Chem., Int. Ed.* **2015**, *54*, 7332.
[29] Z. Xiang, Z.-Y. Wang, T.-B. Ren, W. Xu, Y.-P. Liu, X.-X. Zhang, P. Wu, L. Yuan, X.-B. Zhang, *Chem. Commun.* **2019**, *55*, 11462.
[30] H. Liu, S. Yan, R. Huang, Z. Gao, G. Wang, L. Ding, Y. Fang, *Chem. - Eur. J.* **2019**, *25*, 16732.
[31] B. Tang, C. Wang, Y. Wang, H. Zhang, *Angew. Chem., Int. Ed.* **2017**, *56*, 12543.
[32] R. Huang, C. Wang, Y. Wang, H. Zhang, *Adv. Mater.* **2018**, *30*, 1800814.
[33] B. Liu, Q. Di, W. Liu, C. Wang, Y. Wang, H. Zhang, *J. Phys. Chem. Lett.* **2019**, *10*, 1437.
[34] R. Huang, B. Liu, C. Wang, Y. Wang, H. Zhang, *J. Phys. Chem. C* **2018**, *122*, 10510.
[35] R. Huang, B. Tang, K. Ye, C. Wang, H. Zhang, *Adv. Opt. Mater.* **2019**, *7*, 1900927.
[36] B. Tang, H. Liu, F. Li, Y. Wang, H. Zhang, *Chem. Commun.* **2016**, *52*, 6577.
[37] M. Mandal, T. Chatterjee, A. Das, S. Mandal, A. Sen, M. Ta, P. K. Mandal, *J. Phys. Chem. C* **2019**, *123*, 24786.
[38] S. Hayashi, T. Koizumi, N. Kamiya, *ChemPlusChem* **2019**, *84*, 247.
[39] E. Cho, J. Choi, S. Jo, D.-H. Park, Y. K. Hong, D. Kim, T. S. Lee, *ChemPlusChem* **2019**, *84*, 1130.
[40] Y. Okada, M. Sugai, K. Chiba, *J. Org. Chem.* **2016**, *81*, 10922.
[41] M. Shimizu, Y. Takeda, M. Higashi, T. Hiyama, *Angew. Chem., Int. Ed.* **2009**, *48*, 3653.
[42] Lucifer yellow CH, http://omlc.org/spectra/PhotochemCAD/html/065.html (accessed: June 2017).
[43] M. V. Sednev, V. N. Belov, S. W. Hell, *Methods Appl. Fluoresc.* **2015**, *3*, 042004.

